Bulletin of the Seismological Society of America, Vol. 86, No. 3, pp. 821–831, June 1996

Moment-Tensor Summation to Derive the Active Crustal Deformation in Japan

by Anastasia A. Kiratzi and Constantinos B. Papazachos

Abstract The country of Japan and the surrounding area has been divided into 12 seismogenic sources, which belong to five belts with an almost uniform orientation of the stress field. In each one of these sources, the active crustal deformation has been determined, using the summation of the seismic moment tensors of mainly post-1964 earthquakes. The analysis showed that due to the subduction of the Philippine Sea plate beneath the Eurasian plate, the deformation is expressed as compression at a mean direction of N53°W and an average rate of 1.5 cm/yr. The fault-plane solution corresponding to the summed tensor indicates low-angle thrust faulting with the following parameters: strike 226°, dip 21°, and rake 98°. Along the Sagami trough, dextral strike-slip motion is predominant at an average rate of 6 cm/yr. The summed tensor corresponds to a fault-plane solution with strike 291°, dip 73°, and rake 180°. Along the districts of Fukushima, Tohoku, and the Hokkaido Island, the motion of the Pacific plate toward Eurasia causes compression at a mean direction of N65°W and an average rate of 4 cm/yr. The summed tensor corresponds to a fault-plane solution with strike 199°, dip 18°, and rake 81°, that is, low-angle thrust faulting dipping toward the land. This pattern resembles the Hellenic arc, where the deformation is also taken up by motion on low-angle (18°) thrust faults dipping to the north. In the Tohoku district, the rate of motion reaches a value of 8 cm/yr, which is the highest calculated in the whole Japan area. In the inner part of the Japanese islands (along western Honshu and Niigata), the mean P axis is almost horizontal, trending nearly E–W. In western Honshu, the deformation is mainly expressed as dextral strike-slip motion at an average rate of 5 cm/yr in a N59°E direction. The representative fault-plane solution for this area has strike 240°, dip 81°, and rake 173°. At Niigata, the western coast of Hokkaido, and further north at Okushiri, the deformation is taken up as compression at a mean direction of N96°E at an average rate of 2 cm/yr. The summed tensor corresponds to a fault-plane solution with strike 5°, dip 41°, and rake 90°. The calculated directions and rates of motion along the Japanese islands are in good agreement with the expected values from plate-motion models.

Introduction

The Japanese island arc (see Fig. 1) located at the eastern border of the Eurasian plate is bounded to the east by the Pacific plate and to the south by the Philippine Sea plate. The Pacific plate, spreading from the East Pacific Rise, is subducted beneath the Eurasian plate at the Aleutian-Kurile-Japan-Mariana trench system. The Philippine Sea plate, bounded by the Nankai and Sagami troughs and the Izu-Mariana island arc, is moving northwestward and subducts beneath the Eurasian plate.

Most of the large shallow interplate earthquakes in Japan are due to low-angle thrust fault movements resulting from the subduction process, and all occur on the land side of the trench (Ando, 1975). On the other hand, large intraplate earthquakes occur along the islands of Kyushu and Shikoku. A Wadati-Benioff zone with a shallow dip can be recognized only down to a depth of 80 km beneath the eastern Shikoku region and the Kii peninsula (Shiono, 1977; Shiono *et al.*, 1980). Under the southern Kyushu region, however, the Benioff zone goes down to a depth of 200 km. The typical focal mechanism of the earthquakes that occur in this zone is of normal or strike-slip faulting, with the T-axis being parallel to the leading edge of the subducted Philippine Sea slab (Shiono, 1977).

The purpose of this article is to examine the rate of

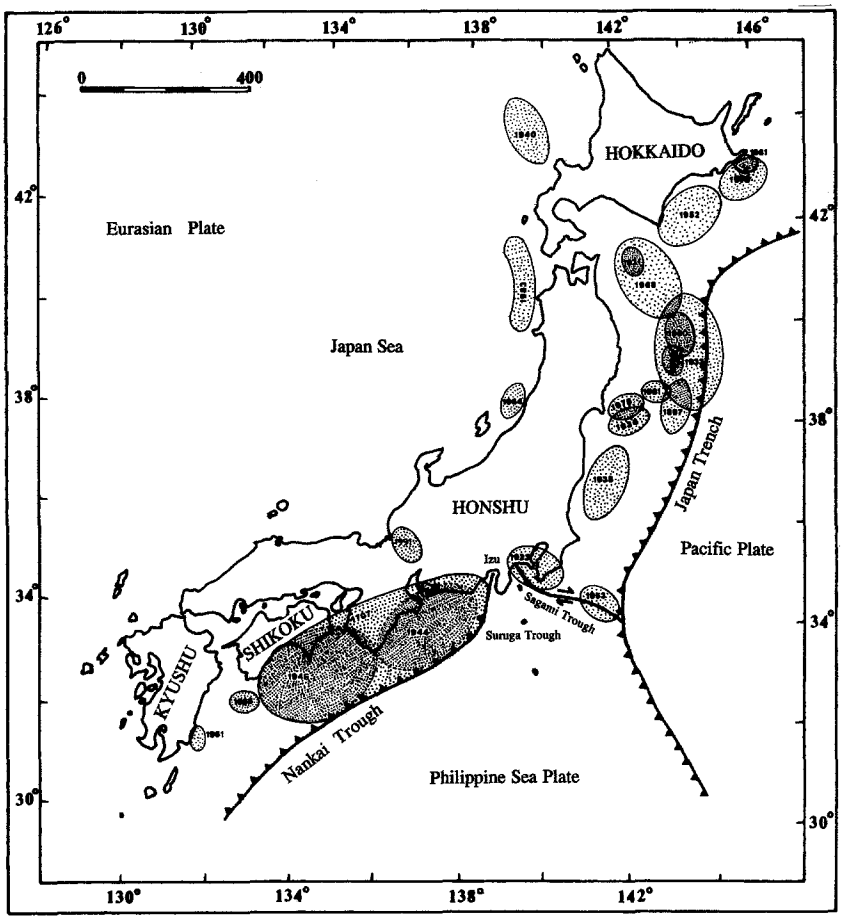

Figure 1. Major tectonic features around the islands of Japan and focal areas of strong and large earthquakes that contributed to the definition of the seismogenic sources (from Papazachos *et al.*, 1994a).

active crustal deformation (upper 20 to 40 km of the lithosphere) in the Japanese islands and the surrounding area and to compare it with the predicted values from plate-motion models. The method of analysis is based on the summation of the moment-tensor elements of well-defined focal mechanisms of shallow earthquakes.

Method of Analysis and Data Used

The method of analysis followed is the one suggested by Papazachos and Kiratzi (1992), which is based on a formulation of Kostrov (1974) and its expansion by Jackson and McKenzie (1988). A detailed description of the procedure is found in Papazachos and Kiratzi (1992), Papazachos *et al.* (1992), Kiratzi (1993), and Kiratzi and Papazachos (1995).

The average strain-rate tensor, $\dot{\varepsilon}_{ij}$, which is the symmetric part of the velocity gradient tensor, is calculated by the following relation (Kostrov, 1974):

$$\dot{\varepsilon}_{ij} = \frac{1}{2\mu V}\frac{\sum_{n=1}^{N} M_{ij}}{T} = \frac{1}{2\mu V}\dot{M}_0\mathbf{F}_{ij} \quad i,j = 1, 2, 3, \quad (1)$$

where V is the deformed volume due to seismic excitation, ΣM_{ij}, is the sum of the moment tensors of the earthquakes that occurred within this volume in T years, μ is the rigidity of crustal rocks ($\mu = 3 \times 10^{11}$ dyn/cm^2), $\dot{M}_0$ is the seismic moment rate, and $\mathbf{F}_{ij}$ is a tensor calculated by the following relation:

$$\mathbf{F}_{ij} = \frac{\sum_{n=1}^{N} M_0^n \mathbf{F}_{ij}^n}{\sum_{n=1}^{N} M_0^n}, \quad (2)$$

where N is the number of all focal mechanisms available; M_0^n is the scalar moment of the nth focal mechanism, and $\mathbf{F}_{ij}^n$ is a function of the strike, dip, and rake of this focal mechanism (Aki and Richards, 1980).

Equation (2) shows that the tensor, $\mathbf{F}_{ij}$, is a moment-normalized tensor, that is, a moment-weighted average of the $\mathbf{F}_{ij}^n$ tensors. This practically means that for areas where the number of focal mechanisms is limited, a single large earthquake will totally control the calculation of $\mathbf{F}_{ij}$ because of its large scalar moment. Therefore, one might consider alternative weighting factors for the $\mathbf{F}_{ij}$ (and not M_0), in order to avoid such problems. In this article, a simple average $\sum_{n=1}^{N} \mathbf{F}_{ij}^n/N$ of the $\mathbf{F}_{ij}^n$ tensors is considered, which translates into attributing equal importance to all the available focal

mechanisms. This is justified, since all the used focal mechanisms have magnitudes $M_S \geqq 5.5$ (and in most cases $\geqq 6.0$) and, therefore, can be considered to represent the regional (and not a local) stress field.

The annual seismic moment release, $\dot{M}_0$, used in equation (1) can be calculated either from a simple averaging of the scalar seismic moments of the earthquakes, over a magnitude threshold for a long enough period of time, or from Molnar (1979):

$$\dot{M}_0 = \frac{A}{1 - B} \cdot M_{0,\max}^{(1-B)}, \tag{3}$$

where $M_{0,\max}$ is the scalar moment of the largest ever observed earthquake in the region, and

$$A = 10^{[a+(bd/c)]} \text{ and } B = \frac{b}{c}, \tag{4}$$

where a and b are the constants of the Gutenberg–Richter relation and c and d are the constants of the moment-magnitude relation applicable to the area:

$$\log M_0 = cM + d. \tag{5}$$

If one uses the simple averaging of seismic moments, it is necessary to have a complete record of seismicity, say for example, all earthquakes over M 6.0 for a time period considerably longer than the repeat time of the large earthquakes. It is true, though, that usually we only know the largest events of the historical times with an accuracy in the magnitude of about 0.4. So a simple average of seismic moments is not always a reliable procedure. Using Molnar's formula, however, one can use a complete record of seismicity, at least for the present century, and consider as $M_{\max}$ the maximum magnitude observed in the historical or in the present century of seismicity. In this article, we adopted and present the results using seismic moment rates calculated by the Molnar formula.

Finally, the integrated rates of motion, U_{ij}, normal and parallel to the zone boundary as well as vertically are calculated by the following relations:

$$U_{11} = \frac{1}{2\mu l_2 l_3} \dot{M}_0 \bar{\mathbf{F}}_{11}, \; U_{22} = \frac{1}{2\mu l_1 l_3} \dot{M}_0 \bar{\mathbf{F}}_{22}, \tag{6}$$

$$U_{33} = \frac{1}{2\mu l_1 l_2} \dot{M}_0 \bar{\mathbf{F}}_{33},$$

$$U_{12} = \frac{1}{\mu l_1 l_3} \dot{M}_0 \bar{\mathbf{F}}_{12} \tag{7}$$

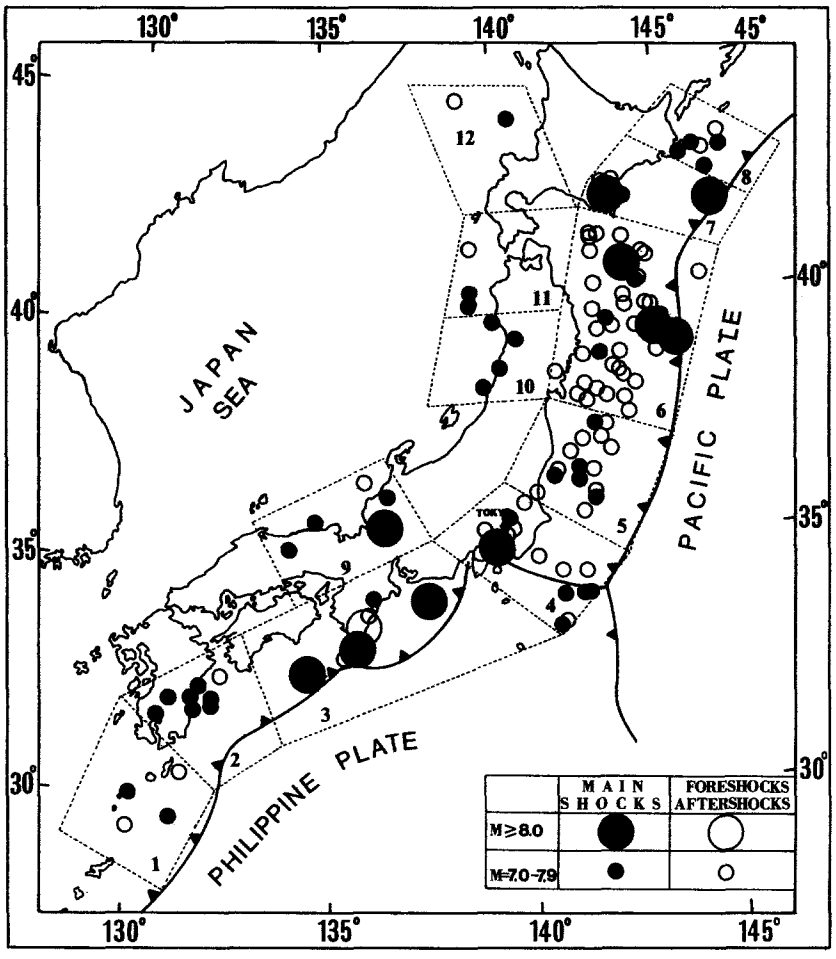

Figure 2. The 12 seismogemic sources into which Japan and its surrounding area has been divided, along with the epicenters of strong ($M_S \geqq 7.0$) shallow mainshocks (black circles) and foreshocks or aftershocks (from Papazachos *et al.*, 1994a).

Table 1
Information on the Basic Parameters Used for Every Source

Seismogenic Source	M^*_{max}	l_1 (km)	l_2 (km)	Az°	b^*	a^*	$\dot{M}_0$ dyne-cm/yr
1: Ryukyu Islands	7.4	305	155	20	1.04	5.80	0.51×10^{26}
2: Kyushu	7.6	305	155	60	1.04	6.08	1.20×10^{26}
3: Nankai	8.6	440	200	60	1.04	5.99	2.81×10^{26}
4: Sagami	8.0	330	170	115	1.04	6.28	2.91×10^{26}
5: Fukushima	7.5	265	170	20	1.04	6.26	1.63×10^{26}
6: Tohoku	8.5	450	230	10	1.04	6.69	1.27×10^{27}
7: S. Hokkaido	8.4	310	100	60	1.04	5.86	1.69×10^{26}
8: N. Hokkaido	7.9	160	95	80	1.04	5.93	1.17×10^{26}
9: W. Honshu	8.4	600	170	60	0.80	4.15	2.24×10^{26}
10: Niigata	7.5	200	80	15	0.80	3.97	0.35×10^{26}
11: Japan Sea	7.7	230	50	10	0.80	4.07	0.60×10^{26}
12: Okushiri	7.6	200	50	155	0.80	3.87	0.32×10^{26}

Values taken from Papazachos *et al.* (1994b). First column gives the code number and the name of every source; M_{max} is the maximum magnitude ever observed in the area; l_1 and l_2 give the length and the width of the deforming zone, respectively; Az is the azimuth in respect to the north of the deforming zone; b and a (annual) are the parameters of the Gutenberg–Richter relation; and $\dot{M}_0$ is the seismic moment rate. The shear modulus was taken $\mu = 3 \times 10^{11}$ dyne/cm^2.

$$U_{13} = \frac{l}{\mu l_1 l_2} \dot{M}_0 \bar{\mathbf{F}}_{13},\ U_{23} = \frac{l}{\mu l_1 l_2} \dot{M}_0 \bar{\mathbf{F}}_{23}, \tag{8}$$

where l_1 and l_2 are the length and the width of the deforming volume, respectively, and l_3 is the depth extent of the seismogenic layer. As it will be stated later, the thickness of the seismogenic layer was taken as $l_3 = 30$ km along the Nankai trough (sources 1 to 4), as $l_3 = 40$ km along the Japan trench (sources 5 to 8), and finally, as $l_3 = 20$ km for the intraplate seismicity (sources 9 to 12). The reference system in equations (1) and (6) to (8) is the zone's local system (length/width/depth). Since $\mathbf{F}_{ij}$ is usually calculated in the north/east/down system (e.g., Aki and Richards, 1980), a rotation in the zone's system is necessary.

It is obvious from the above that the data needed for such an analysis are (a) seismicity data to calculate the parameters of the Gutenberg–Richter relation and the spatial extent of the deforming regions and (b) a set of fault-plane solutions and seismic moments to perform the moment-tensor summations and to calculate the parameters of the moment-magnitude relation.

A catalog that gives information on the earthquakes of the period 1707 to 1992 was used, compiled by Papazachos *et al.* (1994a), and the sources of information for this catalog are referenced in their article. On the other hand, information on the focal mechanisms of mainly post-1964 events in the Japanese islands was taken from published work or from the NEIS and Harvard bulletins.

The whole deforming region was divided into 12 subregions (seismogenic sources) of relatively homogeneous deformation in order to describe the spatial variation in the components of the strain-rate tensor in the area of interest. The subregions of Papazachos *et al.* (1994a) are shown in Figure 2, along with the epicenters of all the shocks with $M_S \geqq 7.0$ that occurred during the period 1840 to 1992. These subregions were determined on the basis of seismotectonic and geomorphological features, on the spatial clustering of the epicenters of strong earthquakes, on the seismicity level, and most importantly, on the distribution of the aftershock volumes and of the source areas of recent and of some well-documented historical earthquakes (see Fig. 1).

Thus, Table 1 gives information on the values of all the parameters used in the calculations, for each seismogenic source separately, while Table 2 gives information on the fault plane solutions and on the seismic moments of the shallow earthquakes used in the moment-tensor summation. These focal mechanisms are shown in Figure 3, grouped for each seismogenic source. From this figure, it is clear that the coverage of focal mechanisms for the 12 seismogenic sources is not always dense. Therefore, the whole area was separated into five belts of similar focal mechanisms, within which the focal mechanism tensor, $\mathbf{F}_{ij}$, was estimated (see Fig. 3 and Table 3). The same $\mathbf{F}_{ij}$ tensor was used for all the sources belonging to the same belt. However, the deformation for each of these sources varies, due to the different moment rates and to the different dimensions of each source.

Parameters c and d of the $\log M_0 - M_S$ relation (equation 5) were determined from the data shown in Figure 4 and listed in Table 2, assuming that the slope of the line (c in equation 5) equals 3/2 (Kanamori and Anderson, 1975; Ekstrom and Dziewonski, 1988). We prefered using this theoretical result, rather than calculate the slope from the original data, since it is quite sensitive, especially to M_S errors. The value of constant d was found equal to 15.99.

The errors involved in an analysis of deformation, using the method followed here, were examined by a Monte Carlo simulation (Papazachos and Kiratzi, 1992). It showed that errors in strain-rate tensor, $\dot{\varepsilon}$, and the velocity values parallel and perpendicular to the plate boundary are mainly controlled by errors in the $\dot{M}_0$ assessment. Errors in $\dot{M}_0$ (and therefore in $\dot{\varepsilon}$ and U) due to errors in a, b, c, d, and $M_{S,max}$ can account for an uncertainty of a factor of about 3. How-

Table 2
Information on the Focal Mechanism Parameters of the Earthquakes Used in the Analysis

Source	Date	h:m	ϕ° N	λ° E	h (km)	M_0	M_S	str	Dip	Rake	Reference
10	31/8/1896	08:06	39.50	140.70	—	1.40×10^{27}	7.2	0	45	90	Thatcher *et al.* (1980)
	1/9/1923	02:58	35.20	139.50	—	2.90×10^{28}	8.0		—		Okal (1992)
9	7/3/1927	09:27	35.60	135.10	10.0	4.60×10^{26}	7.4	155	90	0	Kanamori (1973)
	25/11/1930	19:02	35.10	139.00	5.0	2.70×10^{26}	7.0		—		Abe (1978)
9	20/12/1930		35.00	132.90	20.0		7.0	232	90	180	Ichikawa (1971)
	21/9/1931	02:19	36.15	139.20	—	6.80×10^{25}	7.0				Abe (1975a)
	2/3/1933	17:30	39.25	144.50	30.0	4.30×10^{28}	8.3				Kanamori (1971)
12	1/8/1940	15:08	44.35	139.46	33.0	2.10×10^{27}	7.3	340	46	90	Fukao and Furumoto (1975)
9	10/9/1943	08:36	35.50	134.20	10.0	0.36×10^{27}	7.2	80	90	180	Kanamori (1973)
3	7/12/1944	04:35	33.75	136.00	30.0	15.0×10^{27}	7.8	216	10	90	Kanamori (1972)
9	12/1/1945	18:38	34.70	137.00	—	0.87×10^{26}	7.1	180	30	117	Ando (1974)
3	20/12/1946	19:19	33.10	135.80	30.0	15.0×10^{27}	8.0	205	24	113	Ishibashi (1985)
9	28/6/1948	07:13	36.10	136.20	20.0	0.33×10^{27}	7.1	350	90	0	Kanamori (1973)
	4/3/1952	01:22	42.50	143.00	15.0	6.00×10^{28}	8.3				Okal (1992)
9	19/8/1961	05:33	36.10	136.70	3.0	0.90×10^{26}	6.9	215	60	130	Kawasaki (1975)
9	26/3/1963	02:13	35.80	135.80	—	0.33×10^{26}	6.5	54	68	158	Abe (1974)
1	17/8/1963	11:12	30.60	130.90	39.0	4.70×10^{25}	6.5	35	72	107	Kao and Chen (1991)
2	3/10/1963	23:24	32.20	131.80	34.0	2.6×10^{25}	6.2	32	71	99	Kao and Chen (1991)
11	7/5/1964	07:58	40.39	139.05	22.0	4.30×10^{26}	6.9	211	40	90	Ichikawa (1971)
10	16/6/1964	04:01	38.40	139.30	20.0	3.20×10^{27}	7.5	189	56	90	Abe (1975b)
4	19/4/1965	23:41	34.90	138.30	20.0		6.3	316	56	170	Maki (1974)
5	17/9/1965	16:21	36.35	141.38	31.0		6.7	39	69	90	Kawakatsu and Seno (1983)
5	22/9/1965	22:08	36.40	141.30	42.0		6.6	24	78	90	Kawakatsu and Seno (1983)
5	19/11/1967	12:07	36.50	141.20	39.0		6.0	17	78	90	Kawakatsu and Seno (1983)
1	26/11/1967	00:08	28.60	130.00	30.0	4.60×10^{24}	5.8	47	68	84	Kao and Chen (1991)
2	1/4/1968	00:42	32.50	132.20	31.0	2.30×10^{27}	7.6	43	77	68	Kao and Chen (1991)
2	6/9/1968	19:22	31.00	131.80	52.0	3.30×10^{24}	5.6	51	68	43	Kao and Chen (1991)
2	21/4/1969	07:19	32.20	132.00	31.0	—	6.5	32	68	94	Kao and Chen (1991)
9	9/9/1969	05:15	35.80	137.10	29.0	3.50×10^{25}	6.6	330	90	0	Mikumo (1973)
2	17/9/1969	18:40	31.10	131.40	40.0	1.40×10^{25}	6.4	38	70	77	Kao and Chen (1991)
	25/7/1970	22:41	32.18	131.70	30.0	0.41×10^{27}	7.0				Pacheco and Sykes (1992)
2	26/7/1970	07:10	32.30	131.80	31.0	2.60×10^{25}	6.1	32	68	94	Kao and Chen (1991)
10	16/10/1970	05:26	39.20	140.70	37.0	—	6.2	171	46	119	Mikumo (1974)
2	25/5/1971	13:00	31.30	131.30	40.0	—	5.7	38	70	77	Kao and Chen (1991)
2	29/5/1971	08:52	31.40	131.40	40.0	—	5.7	38	70	77	Kao and Chen (1991)
1	27/11/1971	13:45	29.20	130.10	41.0	—	5.7	21	62	93	Kao and Chen (1991)
1	2/9/1972	01:49	29.40	130.60	24.0	2.60×10^{25}	6.4	197	64	86	Kao and Chen (1991)
1	23/3/1973	19:42	29.30	130.40	36.0	4.3×10^{24}	5.7	32	73	84	Kao and Chen (1991)
8	17/6/1973	03:55	43.10	145.70	30.0	6.7×10^{27}	7.7	238	34	102	Shimazaki (1974)
4	8/5/1974	23:33	34.60	138.80	10.0	5.9×10^{25}	6.9	308	80	190	Abe (1978)
5	8/7/1974	05:45	36.40	141.20	40.0	—	6.3	27	66	78	Kawakatsu and Seno (1983)
9	21/4/1975	17:35	33.18	131.33	9.3	3.4×10^{25}	6.4	305	88	30	Hatanaka and Shimazaki (1988)
4	17/8/1976		34.80	139.00	—	—	5.4	304	82	173	Abe (1978)
4	14/1/1978	03:24	34.74	139.07	11.0	1.1×10^{26}	7.0	270	85	188	Shimazaki and Somerville (1979)
4	14/1/1978	22:31	34.85	138.64	15.0	6.8×10^{24}	5.9	302	79	178	cmt_Harvard solution
6?	20/2/1978	04:37	38.45	141.96	48.0	7.0×10^{25}	6.4	(30	17	106)	cmt_Harvard solution
1	22/2/1978	18:00	29.30	130.50	21.0	4.8×10^{24}	5.8	198	73	102	Kao and Chen (1991)
4	6/4/1978	23:29	35.28	140.71	30.0	1.2×10^{25}	6.1	329	14	167	cmt_Harvard solution
	16/5/1978	07:35	40.65	141.04	15.0	1.9×10^{24}	5.5				cmt_Harvard solution
	16/5/1978	08:24	40.94	141.31	15.0	2.3×10^{24}	5.5				cmt_Harvard solution
12	22/5/1978	07:32	43.30	138.90	15.0	4.3×10^{24}	5.9	199	40	98	cmt_Harvard solution
6	12/6/1978	08:14	38.02	142.07	37.7	3.4×10^{27}	7.5	184	14	59	cmt_Harvard solution
6	14/6/1978	11:34	38.30	142.61	25.5	4.4×10^{25}	6.3	175	21	55	cmt_Harvard solution
6	16/6/1978	05:33	38.14	143.64	15.0	5.5×10^{24}	6.0	170	19	44	cmt_Harvard solution
6	21/6/1978	10:54	37.96	142.17	44.8	8.7×10^{24}	5.9	182	27	75	cmt_Harvard solution
5	27/6/1978	19:10	37.18	143.13	15.0	5.2×10^{24}	6.0	190	16	66	cmt_Harvard solution
	19/1/1979	11:56	41.19	143.46	15.0	1.3×10^{24}	5.5				cmt_Harvard solution
6	20/2/1979	06:32	39.77	144.12	14.8	3.5×10^{25}	6.4	187	15	69	cmt_Harvard solution
	11/7/1979	01:58	36.35	141.83	33.2	9.0×10^{24}	5.9				cmt_Harvard solution
6	16/8/1979	11:55	38.40	142.68	15.0	4.2×10^{24}	5.7	182	12	71	cmt_Harvard solution

(*continued*)

Table 2 (Continued)
Information on the Focal Mechanism Parameters of the Earthquakes Used in the Analysis

Source	Date	h:m	ϕ° N	λ° E	h (km)	M_0	M_S	str	Dip	Rake	Reference
6	12/1/1980	15:57	41.52	143.65	15.0	1.9×10^{25}	6.0	212	9	103	cmt_Harvard solution
8	23/2/1980	05:51	43.50	146.60	34.0	5.6×10^{26}	7.0	213	15	89	cmt_Harvard solution
8	23/2/1980	22:38	43.10	146.90	21.0	1.5×10^{25}	5.9	234	26	112	cmt_Harvard solution
4	29/6/1980	07:20	34.45	138.93	15.0	4.7×10^{25}	6.7	171	86	3	cmt_Harvard solution
6	18/1/1981	09:43	38.50	143.10	12.6	5.9×10^{24}	6.0	176	28	51	cmt_Harvard solution
6	18/1/1981	11:46	38.60	143.10	10.4	7.5×10^{24}	6.0	174	28	47	cmt_Harvard solution
6	18/1/1981	18:11	38.60	142.90	20.0	4.3×10^{25}	6.3	177	26	46	cmt_Harvard solution
6	18/1/1981	18:17	38.70	142.80	20.0	3.7×10^{26}	7.1	186	15	70	cmt_Harvard solution
6	19/1/1981	01:14	38.60	143.00	11.3	8.8×10^{25}	6.6	174	32	49	cmt_Harvard solution
6	22/1/1981	19:34	38.30	142.70	20.0	4.8×10^{25}	6.4	175	14	47	cmt_Harvard solution
6	23/1/1981	10:22	38.20	142.90	20.0	1.1×10^{25}	6.1	188	23	66	cmt_Harvard solution
1	18/2/1981		29.40	130.30	41.0	2.3×10^{24}	5.5	21	62	93	Kao and Chen (1991)
1	12/8/1981	05:10	29.50	130.70	36.0	2.2×10^{24}	5.6	42	56	85	Kao and Chen (1991)
4	20/2/1982	19:18	33.70	141.20	29.9	6.1×10^{25}	6.7	214	40	165	cmt_Harvard solution
6	21/3/1982	02:32	42.20	142.50	36.7	2.6×10^{26}	6.7	308	28	93	cmt_Harvard solution
6	31/5/1982	20:13	38.80	142.20	40.5	1.8×10^{25}	6.1	175	27	51	cmt_Harvard solution
5	23/7/1982	14:24	36.40	141.60	27.0	3.9×10^{26}	6.9	203	14	86	cmt_Harvard solution
5	23/7/1982	17:54	36.10	141.90	21.8	1.5×10^{25}	6.4	237	10	110	cmt_Harvard solution
4	28/12/1982	06:37	33.90	139.50	22.5	2.1×10^{25}	6.1	112	88	−178	cmt_Harvard solution
6?	30/4/1983	14:03	41.50	143.80	31.8	3.4×10^{25}	6.5	(200	14	−99)	cmt_Harvard solution
11	26/5/1983	05:03	40.50	139.10	12.6	4.6×10^{27}	7.7	16	27	86	cmt_Harvard solution
11	9/6/1983	12:49	40.30	139.00	19.7	9.6×10^{24}	6.0	19	40	106	cmt_Harvard solution
11	21/6/1983	06:25	41.40	139.10	17.4	1.9×10^{26}	7.1	23	43	94	cmt_Harvard solution
4	3/10/1983	13:33	34.00	139.50	36.6	1.3×10^{25}	6.2	196	84	5	cmt_Harvard solution
1	23/1/1984	07:34	29.30	130.40	13.0	5.9×10^{24}	6.0	261	18	106	Sipkin and Needham (1989)
2	6/8/1984	19:06	32.39	131.95	41.0	1.3×10^{26}	6.9	26	89	70	Kao and Chen (1991)
9	13/9/1984	23:48	35.79	137.49	13.0	2.5×10^{25}	6.4	341	86	3	Sipkin and Needham (1989)
4	18/9/1984	17:02	34.01	141.50	22.0	2.0×10^{26}	6.9	283	8	−131	Sipkin and Needham (1989)
1	1/3/1985		29.20	130.40	38.0	1.9×10^{24}	5.5	231	27	92	Kao and Chen (1991)
	17/6/1985	19:12	30.30	132.70	20.0	3.0×10^{24}	5.6				Kao and Chen (1991)
5	12/8/1985	03:49	37.77	141.77	37.0	5.3×10^{25}	6.4	302	46	154	Sipkin and Needham (1989)
5	12/2/1986	02:59	36.38	141.13	36.0	2.5×10^{25}	6.0	205	26	99	cmt_Harvard solution
1	24/3/1986	02:01	28.50	130.00	15.0	2.8×10^{25}	6.2	206	12	73	cmt_Harvard solution
5	6/2/1987	12:23	37.00	141.70	38.2	4.4×10^{25}	6.3	200	24	84	cmt_Harvard solution
5	6/2/1987	13:16	37.00	141.70	44.0	1.3×10^{26}	6.7	209	25	99	cmt_Harvard solution
2	18/3/1987	03:36	32.03	131.84	36.0	1.2×10^{26}	6.6	348	27	−103	cmt_Harvard solution
5	7/4/1987	00:40	37.36	141.80	31.0	1.1×10^{26}	6.6	203	16	88	cmt_Harvard solution
5	22/4/1987	20:13	37.10	141.40	33.0	1.1×10^{26}	6.7	199	16	84	cmt_Harvard solution
1	4/4/1988	15:43	30.40	131.10	42.2	1.0×10^{25}	6.0	163	27	30	cmt_Harvard solution
7	6/7/1988	15:54	41.70	144.20	36.3	2.5×10^{25}	6.4	232	21	118	cmt_Harvard solution
	3/1/1989	04:41	29.50	131.40	23.9	5.6×10^{24}	5.8				Kao and Chen (1991)
7	22/1/1989	22:20	41.80	144.30	27.7	2.0×10^{25}	6.3	248	20	139	cmt_Harvard solution
6	26/10/1989	17:06	39.80	143.60	22.2	1.1×10^{25}	6.1	174	26	58	cmt_Harvard solution
6	27/10/1989	01:45	39.80	143.70	15.0	4.0×10^{25}	6.4	200	6	99	cmt_Harvard solution
6	29/10/1989	03:09	39.60	143.50	30.4	6.9×10^{24}	6.0	179	27	70	cmt_Harvard solution
6	29/10/1989	05:25	39.60	143.30	29.8	5.8×10^{25}	6.7	182	19	61	cmt_Harvard solution
6	1/11/1989	18:25	39.90	142.80	24.0	1.4×10^{27}	7.4	183	14	69	cmt_Harvard solution
4	20/2/1990	06:53	34.70	139.30	32.2	4.3×10^{25}	6.6	355	79	10	cmt_Harvard solution
5	5/8/1990	03:36	36.24	141.36	38.8	1.5×10^{25}	6.0	205	26	99	cmt_Harvard solution
4	23/9/1990	21:13	33.30	138.60	16.9	7.1×10^{25}	6.5	36	86	−1	cmt_Harvard solution
	7/5/1991	13:09	39.40	144.70	15.0	1.1×10^{25}	6.6				cmt_Harvard solution
4	3/9/1991	08:44	33.70	138.80	15.0	2.8×10^{25}	6.4	210	54	−13	cmt_Harvard solution
6	18/7/1992	08:37	39.40	143.30	15.0	2.7×10^{26}	6.9	183	11	70	cmt_Harvard solution
6	18/7/1992	10:20	39.40	143.00	15.0	4.5×10^{25}	6.3	221	12	127	cmt_Harvard solution
6	29/7/1992	04:30	39.50	143.50	16.0	2.3×10^{25}	6.2	191	8	83	cmt_Harvard solution
12	12/7/1993	13:17	42.85	139.20	16.5	4.7×10^{27}	7.3	0	35	91	cmt_Harvard solution
12	7/8/1993	19:42	42.83	139.84	26.9	3.0×10^{25}	6.3	357	39	85	cmt_Harvard solution

The first column indicates the code number of the seismogenic source where the fault-plane solution was used in the moment-tensor summation. A question mark (?) near the number of the source denotes that the fault plane solution was not used in the moment-tensor summation because it indicated motion totally different from the other solutions of the same source. In the cases of no number in the first column, only the scalar seismic moment of the earthquake was used in the calculation of the moment–magnitude relation.

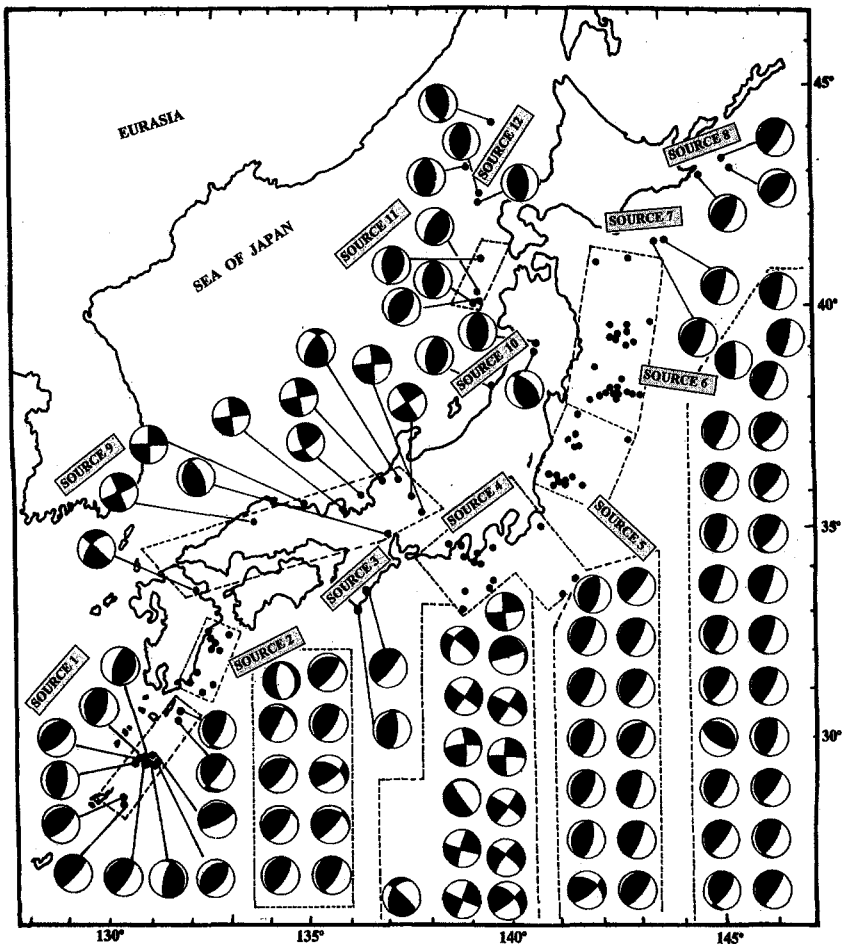

Figure 3. Lower hemisphere equal projection of the focal mechanisms of the earthquakes that were used in the moment-tensor summation for each belt. The dashed lines include the fault-plane solutions for each source. (The parameters of each mechanism are listed in Table 2.)

ever, errors in $\dot{M}_0$ have no effect on the direction of the eigenvector of deformation, which is determined by the tensor $\mathbf{F}_{ij}$. On the other hand, although equation (2) implies that $\mathbf{F}_{ij}$ is affected by errors in the scalar moment, M_0^n, of each event, we do not need to consider these errors since we used a simple averaging scheme for $\mathbf{F}_{ij}$.

The thickness of the seismogenic layer varies between different sources. For the inner sources (9 to 12), we adopted the value of 20 km from the depth distribution of the seismicity. In the outer (external) sources, the depth of the seismicity increases, and there is a gradual transition from shallow to deep seismicity along the subduction. Major events have occurred at depths around 30 km along the Nankai trough (Satake, 1993) and at even greater depths along the Japan trench (Yoshi, 1979; Kawakatsu and Seno, 1983). However, in our case, we have limited the study to the shallow events ($h \leqq 40$ km), and no deeper events were included in the moment-rate calculations. If we had included deeper events, both the thickness of the seismogenic layer and the moment rate would increase, resulting in quite similar deformation velocities. On the other hand, for the deeper events, we would need to follow a different approach and consider a dipping seismogenic layer, as we followed for the intermediate depth (40 to 90 km) seismicity of a different subduction zone (Kiratzi and Papazachos, 1994). Even in such a case, the total thickness of the dipping seismogenic layer does not exceed 30 to 40 km (Yoshi, 1979) along the whole external arc. Therefore, we adopted the value of 30 km for the thickness of the seismogenic layer for the Nankai trough (sources 1 to 4) and 40 km for the Japan trench (sources 5 to 8).

Results and Discussion

The results of the present analysis calculated for each seismogenic source are summarized in Table 3. This table gives the elements of the strain-rate tensor, the fault-plane solution that is derived from the summed moment tensor, the components of the velocity tensor, and the eigensystem of this tensor. In the following, a discussion is made on the results for each one of the five seismic belts into which the area of Japan is divided.

Belt 1: Interplate Seismicity due to the Interaction of the Eurasian and Philippine Sea Plates

This belt consists of three seismogenic sources (1, 2, and 3 in Fig. 2). In total, 24 fault-plane solutions, referenced in Table 2, were used in the moment-tensor summation for this area. The subduction of the Philippine Sea plate underneath the southwestern Japan area takes place in low-angle

Table 3
Results of the Present Analysis for Each Belt

Source	Elements of the strain-rate tensor ($\times 10^{-7}$/yr) in the system 1: North, 2: East, 3: down						Fault-plane solution of the summed moment tensor (Typical focal mechanism for each belt)						
										P		T	
	$\dot{\varepsilon}_{11}$	$\dot{\varepsilon}_{12}$	$\dot{\varepsilon}_{13}$	$\dot{\varepsilon}_{22}$	$\dot{\varepsilon}_{23}$	$\dot{\varepsilon}_{33}$	Strike°	Dip°	Rake°	az°	pl°	az°	pl°
Belt 1							226	21	98	130	24	302	66
1	−0.14	0.14	0.20	−0.18	−0.29	0.32							
2	−0.34	0.34	0.48	−0.42	−0.68	0.76							
3	−0.43	0.43	0.61	−0.53	−0.86	0.96							
Belt 2							291	73	180	155	12	248	12
4	−1.13	1.20	0.19	1.10	−0.46	0.03							
Belt 3							199	18	81	116	27	303	63
5	−0.15	0.28	0.57	−0.68	−0.99	0.83							
6	−0.51	0.96	1.93	−2.28	−3.36	2.79							
7	−0.23	0.43	0.86	−1.01	−1.49	1.24							
8	−0.32	0.60	1.21	−1.43	−2.11	1.75							
Belt 4							240	81	173	106	1	196	11
9	1.03	0.74	−0.18	−1.35	−0.09	0.32							
Belt 5							5	41	90	275	4	96	86
10	−0.11	0.12	−0.02	−1.59	0.25	1.70							
11	−0.26	0.30	−0.06	−3.85	0.60	4.11							
12	−0.16	0.19	−0.03	−2.38	0.37	2.54							

	Elements of the velocity tensor (in mm/yr)						Eigenvalues of the velocity tensor (in mm/yr)								
	U_{11}	U_{12}	U_{13}	U_{22}	U_{23}	U_{33}	λ_1	Az°	Pl°	λ_2	Az°	Pl°	λ_3	Az°	Pl°
1	−3.97	3.14	1.23	−1.86	−1.73	0.97	−6.76	143	15	1.81	81	−61	0.09	46	24
2	−2.94	6.14	2.90	−10.41	−4.08	2.28	−15.28	120	16	3.77	149	−72	0.44	32	−8
3	−4.93	9.72	3.65	−17.38	−5.14	2.87	−24.15	119	13	4.44	157	−74	0.26	31	−10
4	−41.03	39.51	1.12	37.03	−2.77	0.09	−57.62	157	2	53.62	67	−2	0.08	25	87
5	−3.32	5.28	4.58	−10.98	−7.96	3.30	−17.76	118	24	7.32	124	−66	−0.56	29	−2
6	−21.31	34.18	15.48	−47.93	−26.89	11.15	−81.62	124	18	21.73	104	−70	1.81	32	6
7	0.21	2.98	6.87	−21.98	−11.95	4.95	−27.53	102	22	12.07	149	−60	−1.36	20	−20
8	−0.79	11.15	9.70	−23.55	−16.85	6.99	−36.64	114	24	15.97	138	−64	3.32	28	−10
9	36.95	22.24	−0.71	−47.44	−0.35	0.64	−52.94	104	0	42.47	14	−1	0.62	4	89
10	−1.40	−1.27	−0.09	−13.92	1.00	3.40	−14.11	84	−3	3.46	120	86	−1.28	174	−2
11	−5.30	−0.88	−0.23	−19.98	2.41	8.22	−20.23	87	−5	8.43	104	85	−5.26	177	−2
12	−5.67	8.05	−0.14	−17.48	1.49	5.08	−21.63	117	−3	5.19	60	85	−1.64	27	−5

Positive eigenvalues represent dilatation (extension or thickening), and the negative ones represent compression (shortening or thinning). Positive or negative plunge indicates that the eigenvector is directed into or out of the solid earth, respectively.

thrust faults (strike 226°, dip 21°, and rake 98°, see Table 3) and causes the accumulation of strain of up to 10^{-7}/yr. The resulting compressional seismic deformation, due to the seismic excitation, takes place at a mean direction of N53°W and at rates that range from 1 to 2 cm/yr, with an average value of 1.5 cm/yr (see Fig. 5). This result is in good agreement with the results of plate-motion models in this area that indicate that the convergence of the Philippine Sea plate relative to the Eurasian plate takes place in a direction of N50°W and at a rate of about 4 to 5 cm/yr (Seno *et al.*, 1993). It is evident that the Philippine Sea plate subducts obliquely beneath the Eurasian plate. The calculated vertical movements range from 1 to 4 mm/yr along the coastal area of Kyushu and southern Shikoku.

Belt 2: Sagami Trough

The Sagami trough consists of the seismogenic source 4 (see Fig. 2), which includes the focal areas of the 1923 Kanto and the 1953 Boso-oki earthquakes (Fig. 1). Fourteen fault-plane solutions were used in the analysis, and all of them indicate dextral strike-slip motion along the strike of the trough (strike 291°, dip 73°, and rake 180°, see Table 3). Strain is released at about the same rate as above, and the motion parallel to the average fault strike takes place at a rate of about 6 cm/yr.

Belt 3: Interplate Seismicity due to Interaction of the Eurasian and Pacific Plates

This belt includes four seismogenic sources (5, 6, 7, and 8 in Fig. 2). A total number of 43 fault-plane solutions were used in the moment-tensor summation. The subduction of the Pacific plate underneath northeastern Japan causes compressional strain release at rates up to 3×10^{-7}/yr and takes place at low-angle thrust faults that dip to the land (strike 199°, dip 18°, and rake 81°, see Table 3). The compressional deformation takes place in a mean direction of N65°W and at an average rate of 4 cm/yr. In detail, the calculated rate of motion is 2 cm/yr at Fukushima and 3 to 4 cm/yr at south-

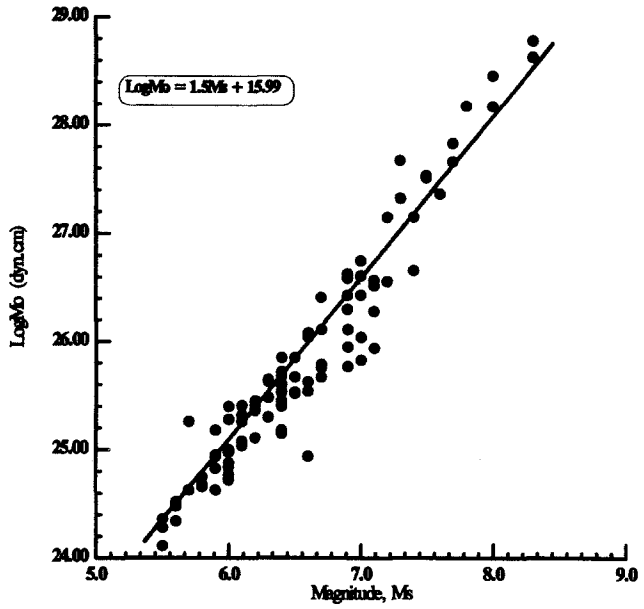

Figure 4. The seismic moment–magnitude relation applicable to the shallow seismicity in Japan. (The data are listed in Table 2.)

ern and northern Hokkaido to reach a value of 8 cm/yr at Tohoku. In all four seismogenic sources, rates of motion associated with the vertical component (thickening of the seismogenic layer) are taking place at about 14 mm/yr.

The pole of rotation of the Pacific plate relative to the Eurasian plate of DeMets *et al.* (1990) predicts convergence in an about a N60°W direction at a rate of 9.59 cm/yr, in good agreement with the results of this article.

Belt 4: Intraplate Seismicity of Western Honshu

Western Honshu includes the seismogenic source 9 (see Fig. 2). Ten fault-plane solutions were used in the moment-tensor summation. The motion takes place in a dextral strike-slip fault (strike 240°, dip 81°, and rake 273°, see Table 3), at a rate of about 5 cm/yr (see Fig. 5).

Belt 5: Intraplate Seismicity in Niigata, Okushiri

This belt includes three seismogenic sources (10, 11, and 12, see Fig. 2). Eleven fault-plane solutions were used for the calculation of the summed tensor, for this belt, that includes Niigata, the western coast of Honshu, and Okushiri. The deformation is rather uniform and is expressed as nearly E–W compression, in a mean direction of N96°E and an

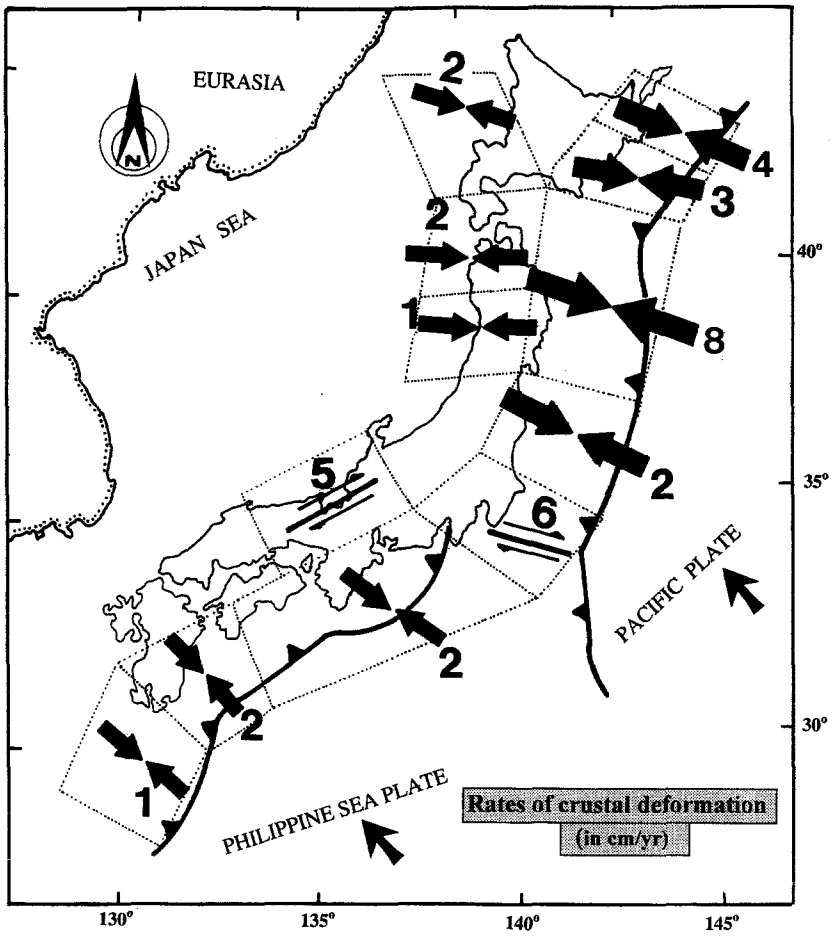

Figure 5. Schematic representation of the seismic crustal deformation rates (in cm/yr) for each seismogenic source.

average rate of 18 mm/yr. The rate of strain release reaches up to 4×10^{-7}/yr. These results are in quite good agreement, within the expected error limits, with the work of Wesnousky *et al.* (1982) who calculated a shortening rate of 11.1 mm/yr at a direction of 100°. The vertical crustal thickening of the upper 20 km of the crust, of this intraplate belt, takes place at rates that range from 3 to 8 mm/yr (see Table 3, component U_{33}). If we assume that this is about 70% isostatically compensated, it would result in about 1 to 2 mm/yr of observable uplift. The Quaternary (last 1 to 3 m.y.) uplift in this area is on average greater than 500 m (Research Group for Quaternary Tectonic Map of Japan, 1973), which would require a rate of uplift of the order of 2 to 6 mm/yr. This difference in the uplift rate estimates is probably due to the fact that strain thickening of the lithosphere beneath the seismogenic layer plays a significant role in the process of the uplift (Wesnousky *et al.*, 1982). One can also notice that in this region, situated in the inner part of the Japan trench, the deformation is occurring at considerably lower rates compared with the ones calculated for the outer interplate part of the interaction of the Eurasian and Pacific plates. It is possible that this difference in the magnitude of motion intensifies previous suggestions of a pre-existing fracture area by which the Japan Sea lithosphere is separated from the northern Japan arc (Fukao and Furumoto, 1975).

Acknowledgments

The authors wish to express their sincere gratitude to Prof. B. Papazachos as well as to their colleagues G. Karakaisis and E. Papadimitriou for stimulating discussions. Part of this work was supported by EPPO (Project 8113/93).

References

Abe, K. (1974). Fault parameters determined by near- and far-field data: the Wakasa Bay earthquake of March 26, 1963, *Bull. Seism. Soc. Am.* **64,** 1369–1382.

Abe, K. (1975a). Static and dynamic fault parameters of the Saitama earthquake of July 1, 1968, *Tectonophysics* **27,** 223–238.

Abe, K. (1975b). Reexamination of the fault model for the Niigata earthquake of 1964, *J. Phys. Earth* **23,** 349–366.

Abe, K. (1978). Dislocations, source dimensions and stresses associated with earthquakes in the Izu peninsula, Japan, *J. Phys. Earth* **26,** 253–274.

Aki, K. and P. Richards (1980). *Quantitative Seismology: Theory and Methods,* Freeman Co., San Francisco, 557 pp.

Ando, M. (1974). Faulting in the Mikawa earthquake of 1945, *Tectonophysics* **22,** 173–186.

Ando, M. (1975). Source mechanisms and tectonic significance of historical earthquakes along the Nankai Trough, Japan, *Tectonophysics* **27,** 119–140.

DeMets, C., R. Gordon, D. Argus, and S. Stein (1990). Current plate motions, *Geophys. J. Int.* **101,** 425–478.

Ekström, G. and A. Dziewonski (1988). Evidence of bias in estimations of earthquake size, *Nature* **332,** 319–323.

Fukao, Y. and M. Furumoto (1975). Mechanism of large earthquakes along the eastern margin of the Japan Sea, *Tectonophysics* **27,** 247–266.

Hatanaka, Y. and K. Shimazaki (1988). Rupture process of the 1975 central Oita, Kyushu, Japan, earthquake, *J. Phys. Earth* **36,** 1–15.

Ichikawa, M. (1971). Reanalysis of mechanism of earthquakes which occurred in and near Japan, and statistical studies on the nodal plane solutions obtained, 1929–1968, *Geophys. Mag.* **35,** 207–273.

Ishibashi, K. (1985). Specification of a soon-to-occur seismic faulting in the Tokai district, central Japan, based upon seismotectonics, in *Earthquake Prediction, an International Review,* D. Simpson and P. Richards (Editors), 297–332.

Jackson, J. and D. McKenzie (1988). The relationship between plate motions and seismic moment tensors, and the rates of active deformation in the Mediterranean and Middle East, *Geophys. J. Int.* **93,** 45–73.

Kanamori, H. (1971). Seismological evidence for a lithospheric normal faulting—The Sanriku earthquake of 1933, *Phys. Earth Planet. Interiors* **4,** 289–300.

Kanamori, H. (1972). Determination of effective tectonic stress associated with earthquake faulting, The Tottori earthquake of 1943, *Phys. Earth Planet. Interiors* **5,** 426–434.

Kanamori, H. (1973). Mode of strain release associated with major earthquakes in Japan, *Ann. Rev. Earth Planet. Sci.* **1,** 213–239.

Kanamori, H. and D. Anderson (1975). Theoretical basis of some empirical relations in seismology, *Bull. Seism. Soc. Am.* **65,** 1073–1095.

Kao, H. and W. Chen (1991). Earthquakes along the Ryukyu-Kyushu Arc: strain segmentation, lateral compression, and the thermomechanical state on the plate interface, *J. Geophys. Res.* **96,** 21443–21485.

Kawakatsu, H. and T. Seno (1983). Triple seismic zone and the regional variation of seismicity along the Northern Honshu arc, *J. Geophys. Res.* **88,** 4215–4230.

Kawasaki, T. (1975). The focal process of the Kita-Mino earthquake of August 19, 1961 and its relationship to a Quaternary fault, the Hatogayukoike fault, *J. Phys. Earth* **24,** 227–250.

Kiratzi, A. (1993). A study on the active crustal deformation of the North and East Anatolian Fault Zones, *Tectonophysics* **225,** 191–203.

Kiratzi, A. and C. Papazachos (1995). Active crustal deformation from the Azores triple junction to Middle East, *Tectonophysics* **243,** 1–24.

Kostrov, B. (1974). Seismic moment and energy of earthquakes, and seismic flow of rock, *Izv. Acad. Sci. USSR Phys. Solid Earth* **1,** 23–40.

Maki, T. (1974). On the earthquake mechanism of the Izu-Hanto-Oki earthquakes of 1974, *Spec. Bull. Earth. Res. Inst. Univ. Tokyo* **14,** 23–36.

Mikumo, T. (1973). Faulting mechanism of the Gifu earthquake of Sept. 9, 1969 and some related problems, *J. Phys. Earth* **21,** 191–212.

Mikumo, T. (1974). Some considerations on the faulting mechanism of the southeastern Akita earthquake of October 16, 1970, *J. Phys. Earth* **22,** 87–108.

Molnar, P. (1979). Earthquake recurrence intervals and plate tectonics, *Bull. Seism. Soc. Am.* **69,** 115–133.

Okal, E. (1992). Use of the mantle magnitude M_m for the reassessment of the moment of historical earthquakes. I: shallow events, *Pageoph* **132,** 17–57.

Pacheco, J. and L. Sykes (1992). Seismic moment catalog of large shallow earthquakes, 1900 to 1989, *Bull. Seism. Soc. Am.* **82,** 1306–1349.

Papazachos, C. and A. Kiratzi (1992). A formulation for reliable estimation of active crustal deformation and its application to central Greece, *Geophys. J. Int.* **111,** 424–432.

Papazachos, C., A. Kiratzi, and B. Papazachos (1992). Rates of active crustal deformation in the Aegean and the surrounding area, *J. Geodyn.* **16,** 147–179.

Papazachos, B., E. Papadimitriou, G. Karakaisis, and T. Tsapanos (1994a). An application of the time- and magnitude-predictable model for the long-term prediction of strong shallow earthquakes in the Japan area, *Bull. Seism. Soc. Am.* **84,** 426–437.

Papazachos, B., E. Papadimitriou, G. Karakaisis, and D. Panagiotopoulos (1994b). Long term earthquake prediction in the circum-Pacific convergent belt, *Pageoph,* 145.

Research Group for Quaternary Tectonic Map (1973). Explanatory text of the Quaternary tectonic map of Japan, Nat. Res. Center for Disaster Prevention, Sci. and Tech. Agency, Tokyo, March 1973.

Satake, K. (1993). Depth distribution of coseismic slip along the Nankai trough, Japan, from joint inversion of geodetic and tsunami data, *J. Geophys. Res.* **98,** 4553–4565.

Seno, T., S. Stein, and A. Gripp (1993). A model for the motion of the Philippine Sea plate consistent with NUVEL-1 and geological data, *J. Geophys. Res.* **98,** 17941–17948.

Shimazaki, K. (1974). Nemuro-Oki earthquake of June 17, 1973: a lithospheric rebound at the upper half of the interface, *Phys. Earth Planet. Interiors* **9,** 314–327.

Shimazaki, K. and P. Somerville (1979). Static and dynamic parameters of the Izu-Oshima, Japan earthquake of Jan. 14, 1978, *Bull. Seism. Soc. Am.* **69,** 1343–1378.

Shiono, K. (1977). Focal mechanisms of major earthquakes in southwest Japan and their tectonic significance, *J. Phys. Earth* **25,** 1–26.

Shiono, K., T. Mikumo, and Y. Ishikawa (1980). Tectonics of the Kyushu-Ryukyu arc as evidenced from seismicity and focal mechanism of shallow to intermediate-depth earthquakes, *J. Phys. Earth* **28,** 17–43.

Sipkin, S. and R. Needham (1989). Moment-tensor solutions estimated using optimal filter theory: global seismicity, 1984–1987, *Phys. Earth Planet. Interiors* **57,** 233–259.

Thatcher, W., T. Matsuda, T. Kato, and J. Rundle (1980). Lithospheric loading by the 1896 Riukuyu earthquake in northern Japan: implications for plate flexure and asthenospheric rheology, *J. Geophys. Res.* **85,** 6429–6435.

Wesnousky, S., C. Scholz, and K. Shimazaki (1982). Deformation of an island arc: rates of moment release and crustal shortening in intraplate Japan determined from seismicity and Quaternary fault data, *J. Geophys. Res.* **87,** 6829–6852.

Yoshi, T. (1979). A detailed cross-section of the deep seismic zone beneath northeastern Honshu, Japan, *Tectonophysics* **55,** 349–360.

Geophysical Laboratory
University of Thessaloniki
GR 540-06
Thessaloniki, Greece

Manuscript received 23 January 1995.